Biosensors and Bioelectronics 145 (2019) 111727

Contents lists available at ScienceDirect

Biosensors and Bioelectronics

journal homepage: http://www.elsevier.com/locate/bios

Co-modified MoO_2 nanoparticles highly dispersed on N-doped carbon nanorods as anode electrocatalyst of microbial fuel cells

Xin Li [a], Meihua Hu [a], Lizhen Zeng [b], Juan Xiong [a], Binhao Tang [a], Zhangmin Hu [a], Lidan Xing [a,c], Qiming Huang [a,c,**], Weishan Li [a,c,*]

[a] School of Chemistry, South China Normal University, Guangzhou, 510006, China
[b] Analysis and Testing Center, South China Normal University, Guangzhou, 510006, China
[c] National and Local Joint Engineering Research Center of MPTES in High Energy and Safety LIBs, Engineering Research Center of MTEES (Ministry of Education), Key Lab. of ETESPG(GHEI), South China Normal University, Guangzhou, 510006, China

ARTICLE INFO

Keywords:
Molybdenum dioxide
Cobalt-modifying
Nitrogen-doping
Carbon nanorods
Anode electrocatalyst
Microbial fuel cell

ABSTRACT

Cobalt-modified molybdenum dioxide nanoparticles highly dispersed on nitrogen-doped carbon nanorods (Co–MoO_2/NCND), are synthesized from anilinium trimolybdate dihydrate nanorods, for the performance improvement of microbial fuel cell based on a mixed bacterial culture. Electrochemical measurements demonstrate that the as-synthesized Co–MoO_2/NCND exhibits excellent electrocatalytic activity for the charge transfer on anode, providing the cell with a maximum power density of $2.06 \pm 0.05\ W\ m^{-2}$, which is strikingly higher than the bare carbon felt anode ($0.49 \pm 0.04\ W\ m^{-2}$). The excellent performance of Co–MoO_2/NCND is ascribed to the increased electronic conductivity of carbon nanorods by N-doping, the high ability of MoO_2 to enrich electroactive bacteria, as demonstrated by high-throughput sequencing, and the enhanced activity of MoO_2 by Co-modifying toward redox reactions in electroactive bacteria. This report provides a new concept of anode electrocatalyst fabrications for the application of microbial fuel cells in electricity generation and wastewater treatment.

1. Introduction

Microbial fuel cells (MFCs) are promising alternatives to the hydrogen-based ones, because they can directly convert various organic substances into electrical energy by using electroactive bacteria (Logan et al., 2019; Lovley, 2006; Zhang et al., 2008). Especially, MFCs are of environmental significance when using organic substances in wastewater as fuels (Liu et al., 2004; Rossi et al., 2018). However, the low output power density is the major obstacle to their practical applications (Chen et al., 2015). Generally, the anode, which provides sites for the charge transfer between fuels and electrode through bacteria, plays a key role in the output power density of MFCs (Cui et al., 2014; Wang et al. 2015; Wang et al., 2018b). Correspondingly, the anode materials should possess good electronic conductivity and electrocatalytic activity toward the redox reactions in bacteria (Xie et al., 2015; Zhou et al., 2011).

Carbon-based materials are usually used in anodes for MFCs, because they possess good chemical stability and electronic conductivity (Li et al., 2017; Zhou et al. 2011; Zhou et al., 2019). Unfortunately, pure carbon-based materials have poor electrocatalytic activity toward the redox reactions in bacteria (Cui et al., 2014; Xiong et al., 2018; You et al., 2017; Zhou et al., 2016). Comparatively, many transition metals oxides or carbides, such as RuO_2, MnO_2, Mo_2C, WC, and WO_3, exhibit better electrocatalytic activity and have been used to modify the carbon-based anodes for improving the output power density of the MFCs (Lv et al., 2012; Rosenbaum et al., 2007; Wang et al. 2013, 2014; Zeng et al., 2010; Zhang et al., 2015; Zou et al., 2016). The improved electrocatalytic activity is related to the redox reactions of transition metal ions in the oxides or carbides, which are fast and exhibit a capacitive behavior (Hu et al., 2019).

Due to the abundance of molybdenum, molybdenum oxides and carbides have received much attention for their applications in MFCs (Yu et al., 2016; Zeng et al., 2018a; Zou et al., 2019). Especially, molybdenum dioxide (MoO_2) presents good electronic conductivity that is required for an electrocatalyst, and excellent biocompatibility that is important for the formation of biofilms on anode (Yang et al., 2016a;

* Corresponding author. School of Chemistry, South China Normal University, Guangzhou 510006, China.
** Corresponding author. School of Chemistry, South China Normal University, Guangzhou 510006, China.
E-mail addresses: huangqm@scnu.edu.cn (Q. Huang), liwsh@scnu.edu.cn (W. Li).

https://doi.org/10.1016/j.bios.2019.111727
Received 17 August 2019; Received in revised form 19 September 2019; Accepted 20 September 2019
Available online 20 September 2019

Zhang et al., 2014). As an anode electrocatalyst of MFCs, however, MoO_2 exhibits poor activity compared to cobalt oxide that is incompatible to bacteria (Mohamed et al., 2017; Zhong et al., 2019). Therefore, an anode based on MoO_2 that simultaneously presents biocompatibility and electrocatalytic activity could be achieved by appropriate modification with cobalt oxide. Recently, Co-doped MoO_2 nanowires have been developed as the electrocatalyst for improving the activity of MoO_2 toward the oxygen reduction reactions (Yang et al., 2017). On the other hand, as support for any electrocatalyst, carbon materials should be highly electronically conductive, which can be accomplished by doping nitrogen (Cheng and Logan, 2007; Wu et al., 2018; Yu et al., 2015).

With the knowledge above, we developed a novel anode electrocatalyst, cobalt-modified molybdenum dioxide nanoparticles highly dispersed on nitrogen-doped carbon nanorods (Co–MoO_2/NCND), for improving output power density of MFCs. The electrocatalytic activity of the resulting Co–MoO_2/NCND was evaluated in a MFC based on mixed bacteria that are easily obtained from the surrounding environment and able to yield electricity (Korneel Rabaey et al., 2003). It is found that the resulting Co–MoO_2/NCND exhibits a significantly improved electrocatalytic activity toward the redox couples in bacteria and provides the MFC with an excellent output power density compared with the commercial carbon felt.

2. Experimental section

2.1. Chemicals and preparations

The synthesis route of Co–MoO_2/NCND is shown in Fig. S1. MoO_2/CND was synthesized by annealing $Mo_3O_{10}(C_6H_8N)_2{\cdot}2H_2O$ nanorods under Ar atmosphere (Liao et al., 2014). Typically, the temperature was kept under 725 °C for 5 h in Ar atmosphere at a flow rate of 20 mL min^{-1}. With this controlled Ar flow rate, the formation of molybdenum carbide can be avoided and the carbon can be kept in the form of nanorods. To obtain $Mo_3O_{10}(C_6H_8N)_2{\cdot}2H_2O$ nanorods, 2 mmol ammonium heptamolybdate was dispersed into 40 mL deionized water, and 3.28 mL aniline was added. Then 1.0 M HCl was added slowly under vigorous stirring until a white precipitate was formed. After stirring at 50 °C for 2 h, the product was filtered, washed with ethanol and dried. To obtain Co–MoO_2/CND, 767.7 mg of the as-prepared MoO_2/CND and 0.5 mmol cobalt acetylacetonate were dispersed into 90 mL deionized water under stirring for 10 h at 80 °C. Subsequently, the mixture was sealed for hydrothermal reaction at 150 °C for 3 h. To obtain Co–MoO_2/NCND, 250 mg of Co–MoO_2/CND and 100 mg dicyanamide were dispersed in 100 mL ethanol under vigorous stirring at room temperature for 6 h and dried. The precipitation was annealed at 450 °C for 1 h, then 650 °C for 2 h in Ar, and harvested by washing with 1.0 M HCl to remove residual Co species. MoO_2/NCND was obtained similarly to Co–MoO_2/NCND but without the hydrothermal reaction of MoO_2/CND with $Co(C_5H_7O_2)_3$. Ammonium heptamolybdate ($(NH_4)_6Mo_7O_{24}{\cdot}4H_2O$, 99.9%), aniline ($C_6H_7N$, 99%), cobalt acetylacetonate ($Co(C_5H_7O_2)_3$, 98%), and dicyanamide ($C_2H_4N_4$, 99%) were purchased from Aladdin Co., China. Hydrochloric Acid (HCl, 36.0–38.0 wt%) was obtained from Sinopharm Chemical Reagent Co., China.

2.2. Physical characterization

X-ray diffractometer (XRD, Rigaku Ultima IV, Japan), scanning electron microscopy (SEM, FEI-quanta-FEG-250, USA), and transmission electron microscopy (TEM, JEOL JEM-2100HR, Japan) were used to identify the crystal structure and morphologies of samples. The surface chemical composition of sample was analyzed by X-ray photoelectron spectroscopy (XPS, Thermo Fisher Scientific, USA). The Raman spectra and confocal laser photofluorogram were collected from Witec Apyron (WITec alpha 300R, Ulm, Germany). The specific surface area and pore size distribution were measured by a porosimetry analyzer (V-Sorb 2800P).

2.3. MFC construction

A single-chamber MFC (28 mL cubic shape) was constructed as previously described (Zeng et al., 2018b). The Co–MoO_2/NCND (loading mass: 1.5 mg cm^{-2}) was dispersed in 5 wt% poly (tetrafluoroethylene) (PTFE) solution and coated on one side of carbon felt (2.0 cm × 2.0 cm) to obtain Co–MoO_2/NCND/CF anode. The MoO_2/CND/CF, Co–MoO_2/CND/CF, MoO_2/NCND/CF and bare CF anodes were also prepared in the same way for comparison. The cathode was prepared using the commercial catalyst of Pt/C (loading mass: 0.5 mg cm^{-2}) as previously described (Zeng et al., 2018b).

Typically, 5.0 mL bacterial inoculum (initially inoculated with and activated anaerobic sludge) and 23 mL medium solution were inoculated in MFCs. The medium solution for the MFCs contains phosphate buffer solution (PBS, 0.05 M, pH 7.3) and sodium acetate (1 g L^{-1}). The PBS (per L) consists of 11.40 g $Na_2HPO_4{\cdot}12H_2O$, 2.77 g $NaH_2PO_4{\cdot}2H_2O$, 0.31 g NH_4Cl, 0.13 g KCl, 12.5 mL vitamin solution, and 12.5 mL trace mineral solution. In a practical application of the fuel cells, a real wastewater (pH 6.3, COD 1650 mg L^{-1}) was collected from a food processing company (Nanfang Tianmei Food Co., Ltd, Guangzhou) to run the fuel cells without adding any other chemical. The efficiency of the cells was evaluated by chemical oxygen demand (COD) analyses.

2.4. Electrochemical measurements

The voltage output data of MFCs were collected from a voltage acquisition instrument (DAQ, PS2024, China). All MFCs were performed in batch mode at 25 °C with an external resistance (1000 Ω) and conducted in triplicate, 60% of the medium solution was refreshed when the output voltage decreased below 0.02 V. After 3 weeks' batch mode operations, linear sweep voltammetry was performed with a scan rate of 1 mV s^{-1} to obtain polarization curves (Wang et al., 2013). The output power density (W m^{-2}) was calculated from P = IU/A, where I (A) is the current, U (V) the cell voltage, and A (m^{-2}) the projected anode area.

Other electrochemical measurements were performed on multichannel potentiostats (Bio-Logic SAS VMP-3, France) in three electrode half-cells containing the anode (working electrode), titanium wire (counter electrode) and saturated calomel electrode (SCE, reference electrode). Chronoamperometry (CA) was performed at a biased potential by 0.2 V (*vs.* SCE) and the current response was recorded. Chronopotentiometry (CP) was performed under 0.1 μA after 3 weeks' batch mode operations. Cyclic voltammetry (CV) was conducted from −0.6 V to 0.3 V (*vs.* SCE) at a scan rate of 1 mV s^{-1}. Electrochemical impedance spectroscopy (EIS) was performed in three-electrode mode or two-electrode mode in a frequency range from 10^5 to 10^{-2} Hz with a potential amplitude of 5 mV when the MFCs at open circuit potential. In the three-electrode mode, the anode was used as working electrode, the cathode as counter electrode, and saturated calomel electrode (SCE) as reference electrode. To obtain total resistance of different MFCs, the two-electrode mode was performed, where the anode as working electrode and the cathode as counter and reference electrodes.

3. Results and discussion

3.1. Structural and morphology of Co–MoO_2/NCND

As shown in Fig. 1a, the crystalline planes of monoclinic MoO_2 (JCPDS 32–0671) can be clearly observed for all samples. The XRD pattern of Co–MoO_2/NCND shows a slight shift to high diffraction angles (inset of Fig. 1a), suggesting that Co and N have been successfully combined into MoO_2/CND. Similar phenomenon was observed for the Fe or Co-doped Mo_2C (Lin et al., 2016; Wan and Leonard, 2015). The Raman spectra in these samples show two dominant peaks at 1350 and

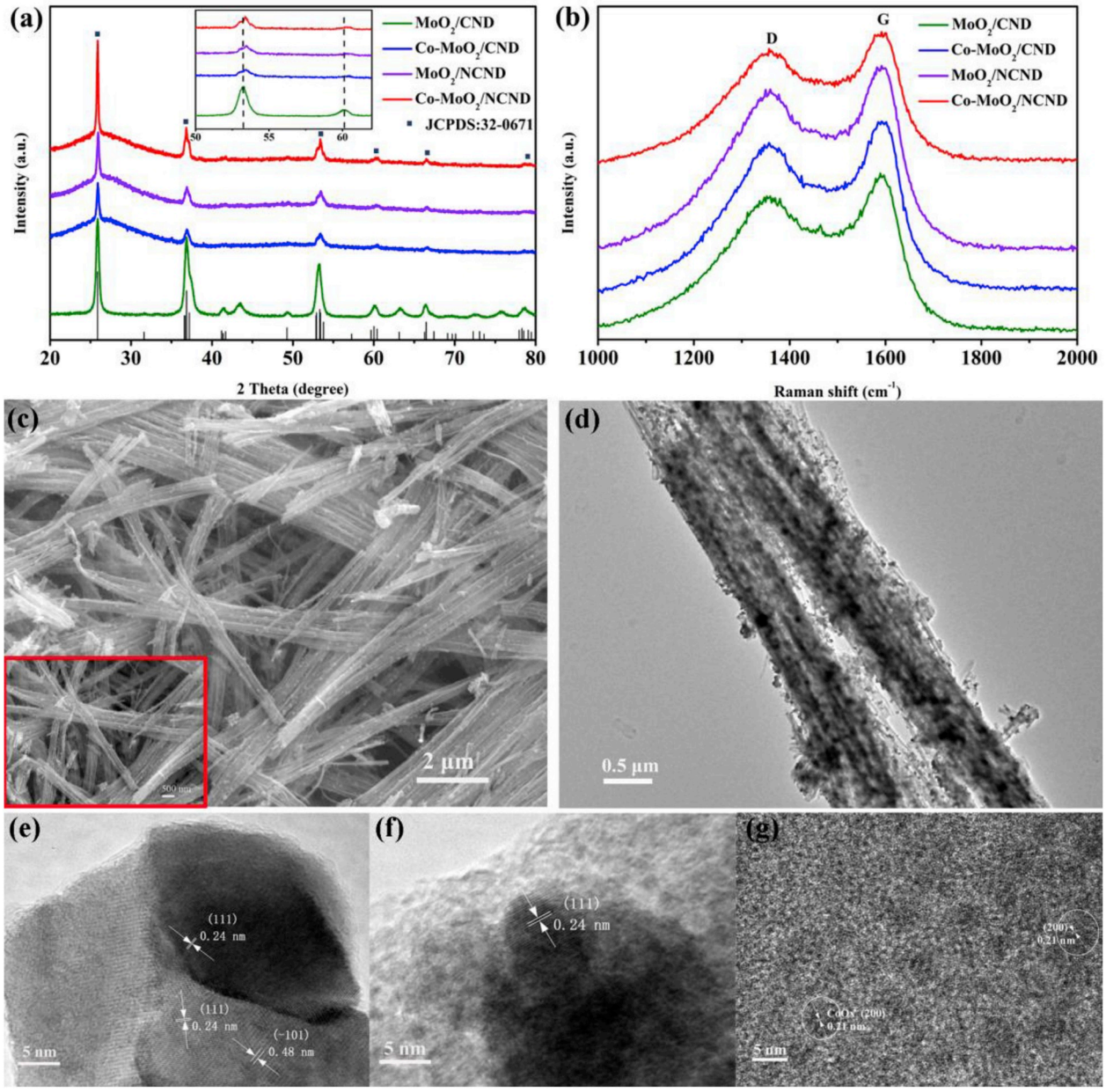

Fig. 1. XRD patterns (a), Raman spectra (b) of MoO_2/CND, Co–MoO_2/CND, MoO_2/NCND and Co–MoO_2/NCND; SEM image (c), TEM image (d) and high-resolution TEM images (e, f, g) of Co–MoO_2/NCND.

1600 cm^{-1} corresponding to D and G bands, respectively (Yang et al., 2016b), indicative of the presence of carbon (Fig. 1b).

Co–MoO_2/NCND presents a morphology of nanorods (Fig. 1c), which apparently inherits from the precursor $Mo_3O_{10}(C_6H_8N)_2{\cdot}2H_2O$ (Fig. S2). The nanorods are about 500 nm in diameter and 5 μm in length (Fig. 1c and Fig. S3). The TEM image clearly shows that there are nanoparticles uniformly dispersed in nanorods (Fig. 1d). As presented in high-resolution TEM images, the nanoparticles on the surface (Fig. 1e) and among (Fig. 1f) nanorods are MoO_2 (about 50 nm) with the fringe spacing of 0.24 nm, corresponding to the (111) lattice plane of MoO_2. Furthermore, it can be clearly seen that CoO (fringe spacing of 0.21 nm) with its particle size of 5 nm in diameter on MoO_2 (Fig. 1g), confirming that MoO_2 has been modified by CoO. To confirm the presence of carbon, MoO_2 was removed by H_2O_2 (30 wt%). The residual carbon maintains the morphology of nanorods (Fig. S4a) and presents an amorphous nature (Fig. S4b). Additionally, Co–MoO_2/NCND provides a larger surface area (58.5 $m^2\,g^{-1}$) (Fig. S5).

As shown in Fig. 2a, Mo, O, C, Co, and N, can be detected in Co–MoO_2/NCND sample from XPS profile. The high resolution Mo 3d spectrum (Fig. 2b) indicates the Mo(IV) characteristic of Mo in MoO_2 (Liu et al., 2014; Wang et al., 2018a). The Co 2p spectrum (Fig. 2c) confirms the presence of Co in the form of oxide (Lin et al., 2016; Wan et al., 2017). The N 1s spectrum (Fig. 2d) and the C 1s spectrum (Fig. S6a) suggest that the N-doping is in the forms of pyridinic and pyrrolic nitrogen (Li et al., 2015). These species contribute to the improved electronic conductivity of the Co–MoO_2/NCND, which can be confirmed by electrochemical impedance spectroscopy (see Section 3.3). The EDS elemental mappings of Co–MoO_2/NCND (Fig. 2e) demonstrate that Co, N, C and Mo are uniformly dispersed in the sample. The weight percent of C in Co–MoO_2/NCND from TGA is 23.7% (Fig. S6b). From EDS (Fig. S6c), the content of Co and N in Co–MoO_2/NCND is 5.8 and 3.0 at%, respectively.

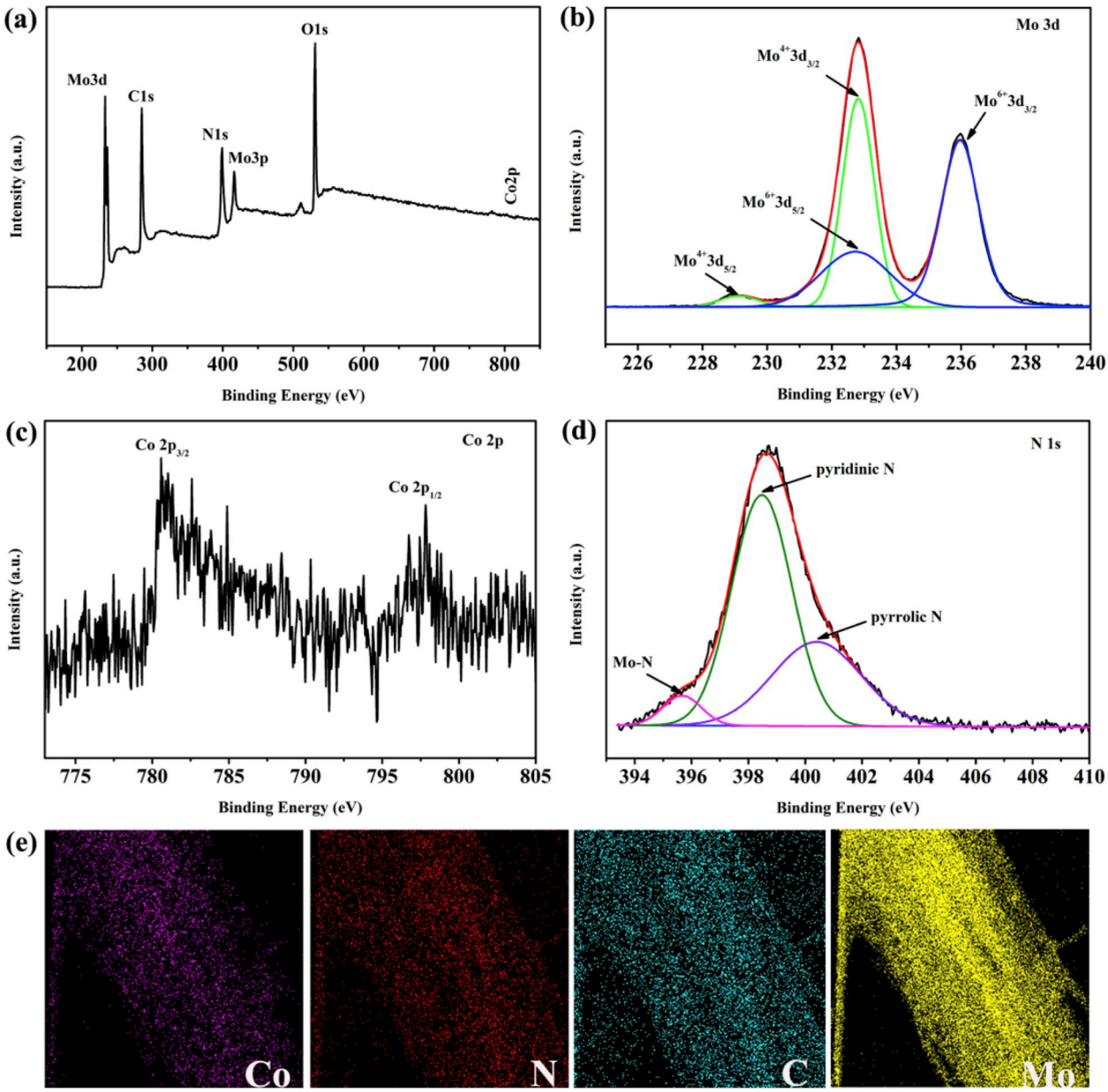

Fig. 2. XPS survey spectrum (a), XPS patterns of Mo 3d (b), Co 2p (c) and N 1s (d), and EDS element mappings (e) for Co–MoO_2/NCND.

3.2. Electrocatalytic activity of Co–MoO_2/NCND/CF anode

The anodes in MFCs were kept at 0.2 V (*vs.* SCE). The current responses are presented in Fig. 3a. The Co–MoO_2/NCND/CF anode delivers the largest current (2.01 ± 0.05 mA cm^{-2}), compared to Co–MoO_2/CND/CF (1.74 ± 0.05 mA cm^{-2}), MoO_2/NCND/CF (1.74 ± 0.04 mA cm^{-2}), MoO_2/CND/CF (1.68 ± 0.07 mA cm^{-2}) and CF (1.01 ± 0.02 mA cm^{-2}). Fig. 3b shows that Co–MoO_2/NCND/CF yields the most negative plateau potential (0.569 ± 0.010 V) after applying constant current (0.1 μA), compared to Co–MoO_2/CND/CF (0.520 ± 0.002 V), MoO_2/NCND/CF (0.528 ± 0.002 V), MoO_2/CND/CF (0.510 ± 0.002 V) and CF (0.480 ± 0.020 V). These results indicate that the Co–MoO_2/NCND/CF exhibits better electrocatalytic activity for the charge transfer between anode and bacteria (Li et al., 2018; Zeng et al., 2018a).

As shown in Fig. S7, all the anodes before biofilm formation do not exist any activity toward the oxidation of acetate. After 3 weeks' batch mode operations, as presented in Fig. 3c, far larger oxidation currents than the reduction currents are observed from all anodes, indicating the continuous electrocatalytic oxidation of acetate by bacteria. The Co–MoO_2/NCND/CF presents a peak oxidation current density (1.51 mA cm^{-2}) at −0.09 V, which is higher than MoO_2/CND/CF anode (0.85 mA cm^{-2} at −0.22 V) and CF anode (0.52 mA cm^{-2} at −0.29 V), indicating the enhanced electrocatalytic activity of the Co–MoO_2/NCND/CF electrode toward the oxidation of acetate through bacteria. When the solution is replaced by that without acetate, two major redox pairs can be observed (Fig. 3d), which result from the electroactive biofilm (Fricke et al., 2008; Katuri et al., 2010). This charge transfer activity is accomplished by the redox couples in bacteria (Guo et al., 2013). The first one at about −0.30 V corresponds to OmcZ, while the second at −0.35 V to OmcB (Liu et al., 2008; Nevin et al., 2009; Peng and Zhang, 2017; Richter et al., 2009; Yuan et al., 2013). The largest current of Co–MoO_2/NCND/CF electrode toward the oxidation of acetate (Fig. 3c) indicates that this electrode exhibits the best electrocatalytic activity for the redox reactions in bacteria.

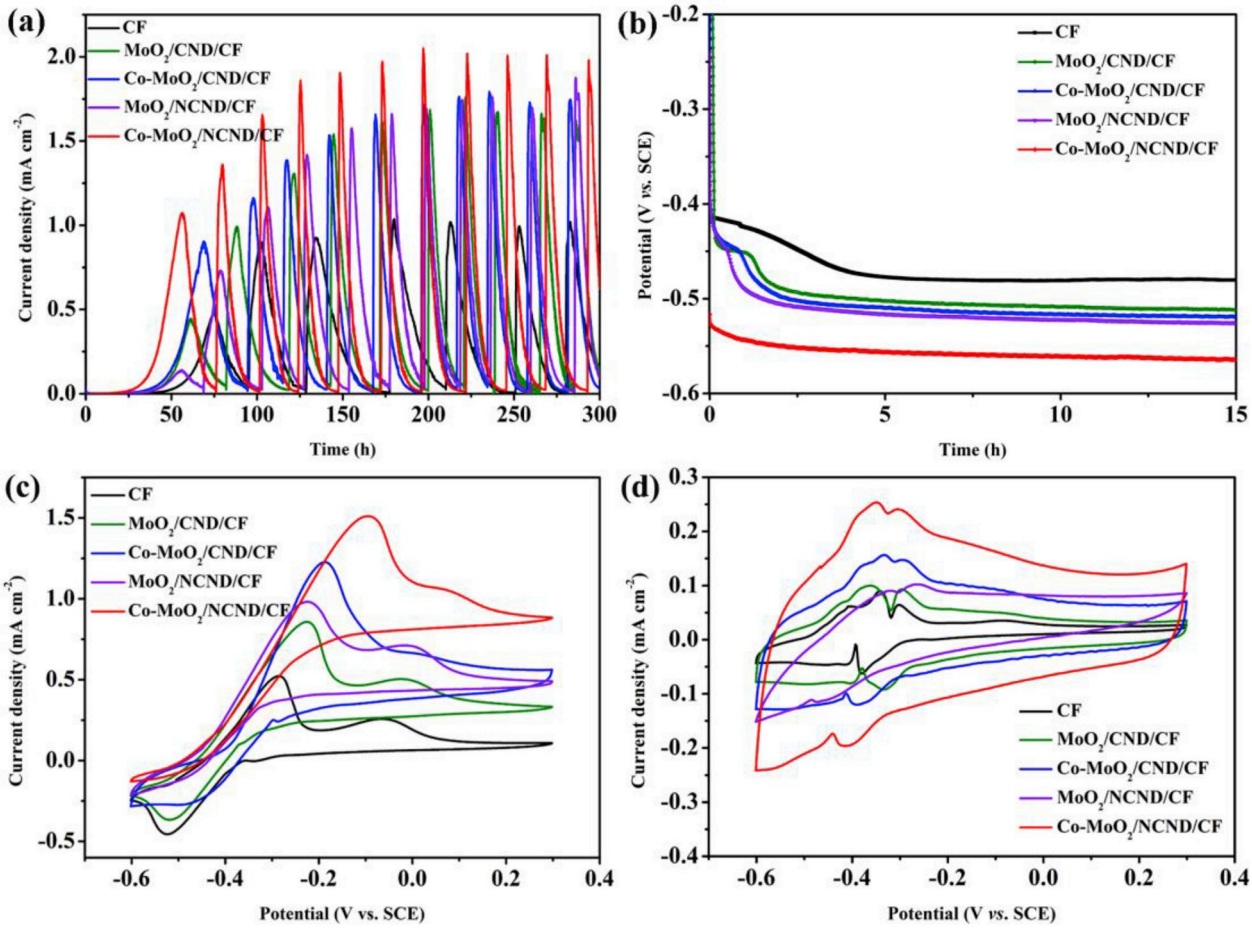

Fig. 3. Current response at 0.2 V (*vs.* SCE) (a) and potential response after 3 weeks' batch mode operations under a constant current of 0.1 μA (b) of different electrodes; Cyclic voltammograms with turnover conditions (the medium solution with 1 g L^{-1} sodium acetate) (c) and without turnover conditions (the medium solution without 1 g L^{-1} sodium acetate) (d) at a scan rate of 1 mV s^{-1} after biofilm growth for different electrodes.

3.3. Performance of MFCs

The performance of Co–MoO_2/NCND/CF as anode was evaluated in a single-chamber MFC with a comparison of other anodes (Fig. 4a). The cells were inoculated with bacterial inoculum and the medium solution containing 1 g L^{-1} acetate. Fig. 4b presents the polarization curves of the MFCs after 3 weeks' batch mode operations. The MFC equipped with Co–MoO_2/NCND/CF anode reveals the largest current density compared with other anodes, indicating that Co–MoO_2/NCND/CF has small polarization, which is consistent with the CP result (Fig. 3b). The overshoot phenomena observed in polarization curves at low voltage result from the insufficient time for bacteria to adapt the high electron flow rate (Mardanpour et al., 2012; Watson and Logan, 2011). It can be found from Fig. 4c that the power density delivered by the MFCs increases in the following order of anodes: CF (0.49 ± 0.04 W m^{-2}), MoO_2/CND/CF (1.21 ± 0.09 W m^{-2}), MoO_2/NCND/CF (1.49 ± 0.05 W m^{-2}), Co–MoO_2/CND/CF (1.61 ± 0.10 W m^{-2}), and Co–MoO_2/NCND/CF (2.06 ± 0.05 W m^{-2}). Apparently, the Co-modifying and the N-doping are beneficial for the performance improvement of the anodes. The Co-modifying enhances the electrocatalytic activity of MoO_2 toward the redox reactions in bacteria, without significantly deteriorating the biocompatibility of anode because of its small content (Mohamed et al., 2017). The N-doping in carbon nanorods increases the electronic conductivity of the carbon, which is necessary for the redox reactions in bacteria on anode (You et al., 2017). As presented in Fig. 4d, the potential changes are similar for cathodes but significantly different for anodes in five cells, indicating that the improved performance of MFCs results from the contribution of the anode rather than cathode. Compared with the anodes recently reported in literature, the Co–MoO_2/NCND/CF anode provides MFC with larger power density (Table S1). Furthermore, the voltage output of the MFC with Co–MoO_2/NCND/CF anode under a fixed external resistance of 1000 Ω is stable in the subsequent batch cycles (Fig. S8), indicating the stability of MFC in long-time operations. With this excellent power generation ability, Co–MoO_2/NCND/CF anodes provide two-series MFCs with sufficient power to run an electronic device (Fig. S9). Especially, the MFC using Co–MoO_2/NCND/CF anode still presents excellent performance when using a real wastewater to replace the acetate medium, as shown in Fig. S10. The cell outputs a maximum voltage of 0.40 ± 0.02 V under a load of 1000 Ω (Fig. S10a), delivers a maximum power density of 1.25 W m^{-2} (Fig. S10b) and yields a COD removal efficiency of 75.6% after one batch operation under a load of 1000 Ω (Fig. S10c).

EIS was performed to further verify the contribution of Co–MoO_2/NCND to the improved performance of MFC. The electrochemical impedance spectra of the different anodes, in three-electrode mode under open circuit potential of the MFCs after 3 weeks' batch mode operations, are presented in Fig. 5a, and the equivalent circuit for fitting these data was inserted in it. The electrochemical impedance spectra consists of the semicircle at high frequency, corresponding to the charge transfer between bacteria and anode, and the linear line at low frequency, corresponding to the Warburg's diffusion impedance (He and Mansfeld, 2009). Fig. 5b presents the Ohmic resistance (R_{ohm}) and the charge transfer resistance (R_{ct}) obtained by fitting. Because of the high ionic conductivity of solution, the obtained R_{ohm} mainly reflects the

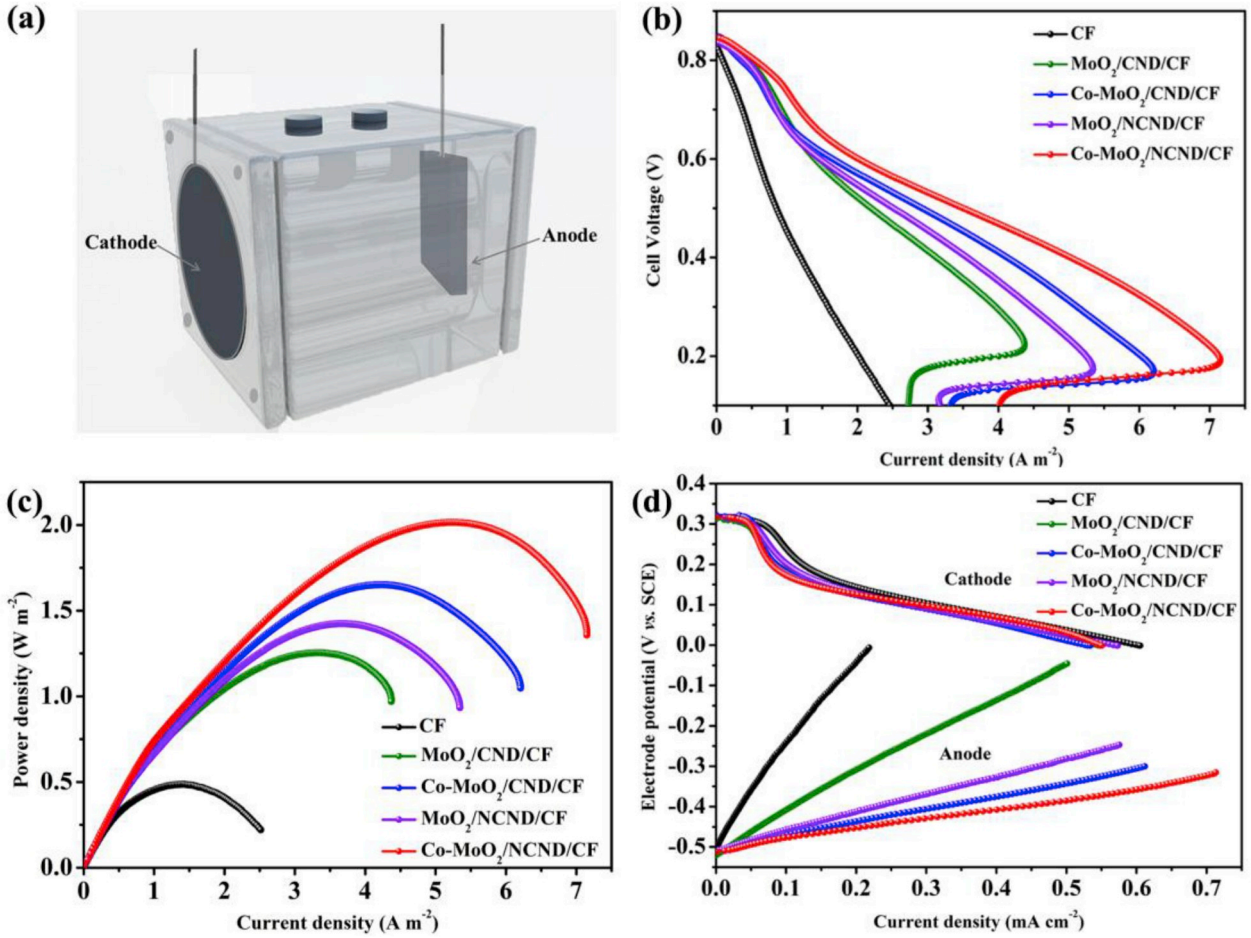

Fig. 4. Schematic illustration of MFC for evaluating anode performance (a); Polarization curves (b), power density (c) and individual potential of electrodes (d) for the MFCs with different anodes after 3 weeks' bath mode operations.

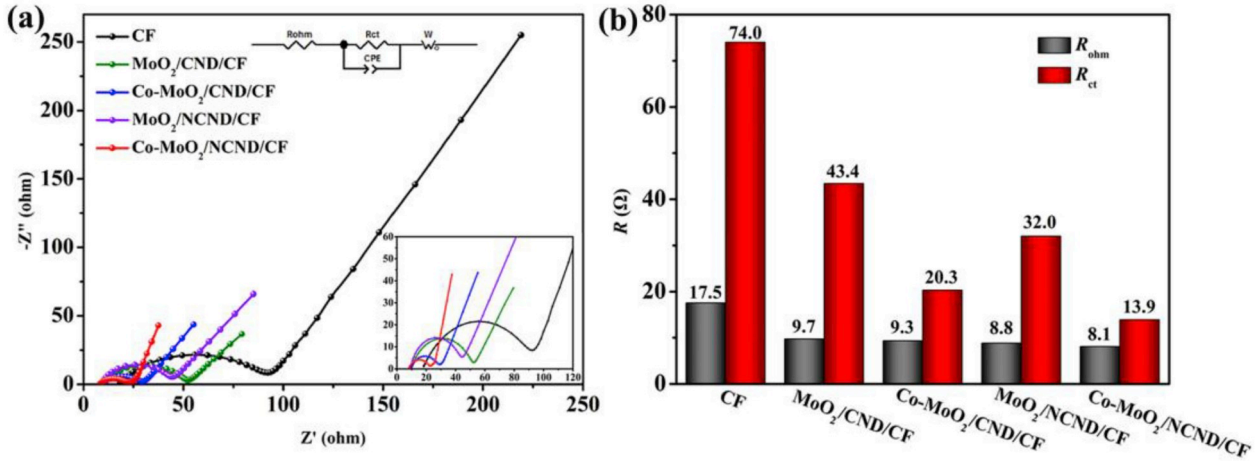

Fig. 5. Electrochemical impedance spectra of different anodes under open circuit potential in MFCs after 3 weeks' batch mode operations (Inset: equivalent circuit for fitting) (a); Corresponding ohmic resistance (R_{ohm}) and charge transfer resistance (R_{ct}) (b).

electronic conductivity of the anodes. MoO_2/NCND/CF has a smaller R_{ohm} (8.8 Ω) than MoO_2/CND/CF (9.7 Ω) and Co–MoO_2/NCND/CF has a smaller R_{ohm} (8.1 Ω) than Co–MoO_2/CND/CF (9.3 Ω), confirming that the electronic conductivity of the carbon in the electrocatalysts has been enhanced by N-doping. Notably, Co–MoO_2/NCND/CF anode has a smaller R_{ct} (13.9 Ω) than Co–MoO_2/CND/CF (20.3 Ω), MoO_2/NCND/CF (32.0 Ω), MoO_2/CND/CF (43.4 Ω) and CF (74.0 Ω), highlighting the superior electrocatalytic activity of Co–MoO_2/NCND. EIS was also performed with the MFCs in two-electrode mode, where the anode was used as working electrode and the cathode as reference and counter electrodes. The obtained results are presented in Fig. S11 and Table S2, which indicate that the MFC using Co–MoO_2/NCND/CF anode has not only the smallest R_{ohm} and R_{ct}, but also the smallest cell internal resistance (R_{total}), confirming the contribution of Co–MoO_2/NCND to the

improved cell performance.

3.4. Biofilm of Co–MoO_2/NCND/CF anode

To accomplish the charge transfer between the anode and bacteria, a biofilm should be formed on anode, which can be confirmed by SEM and Raman spectroscopy observations after operating the MFCs. As presented in Fig. 6a, the thick biofilm densely cover the entire surface of the Co–MoO_2/NCND/CF anode, which is consistent with the photofluorogram (Fig. S12). High-resolution SEM image of the anode shows the rod-shaped bacteria (Fig. 6b). Although the thick biofilms are also formed on other anodes (Fig. S13), the power density achieved by the MFCs based on these anodes is lower than the MFC using the Co–MoO_2/NCND/CF anode, suggesting that the Co–MoO_2/NCND provides MFC with improved power output by enriching electroactive bacteria or by accelerating the charge transfer between anode and bacteria. High-throughput sequencing was performed to detect the component of the bacteria in the biofilms on different anodes. The obtained results are presented in Fig. S14, which show diverse communities on the anodes, including electroactive bacteria (*Geobacter*), biodegradation-related bacteria (*Chrysebacterium*, *Taibaiella, Aquamicrobium, Azoarcus*) (Jia et al., 2013; Zhang et al., 2017). As shown in Fig. S14a, MoO_2/CND/CF has the largest amount of *Geobacter* species, suggesting that MoO_2 is able to enrich electroactive bacteria, but delivers less power density compared to other anodes except for the bare CF (Fig. S14b), indicative of the insufficient electrocatalytic activity of MoO_2 toward the redox reactions in electroactive bacteria. Co–MoO_2/CND/CF has far less *Geobacter* species but delivers larger power density than MoO_2/CND/CF, suggesting that Co is harmful to the enriching of electroactive bacteria but presents excellent electrocatalytic activity toward the redox reactions in electroactive bacteria. N-doping also affects the biocompatibility of anodes but is less harmful than Co-modifying, as indicated by comparing MoO_2/CND/CF with Co–MoO_2/CND/CF and MoO_2/NCND/CF. MoO_2/NCND/CF has less amount of *Geobacter* species but delivers larger power density than MoO_2/CND/CF, suggesting that the enhanced electronic conductivity of the electrocatalyst by N-doping is beneficial for the redox reactions in electroactive bacteria. With the contributions of MoO_2 to the enriching of electroactive bacteria, Co-modification to the improved electrocatalytic activity and N-doping to the enhanced electronic conductivity, Co–MoO_2/NCND/CF anode provides the MFC with excellent output power density by accelerating the redox reactions in bacteria, as illustrated schematically in Fig. 6c.

4. Conclusions

A novel anode electrocatalyst, cobalt-modified molybdenum dioxide nanoparticles highly dispersed on nitrogen-doped carbon nanorods (Co–MoO_2/NCND), has been successfully developed for enhancing the performance of MFCs. MoO_2 presents excellent biocompatibility with electroactive bacteria, especially its ability to enrich electroactive bacteria, Co-modifying enhances its electrocatalytic activity, and N-doping increases the electronic conductivity of carbon nanorods. With these contributions, the resulting anode electrocatalyst provides MFC with excellent power density output. However, more investigations should be made before this anode electrocatalyst is put into practical use. For example, its electrocatalytic activity should be related to the contents of Co and N, which needs further understanding.

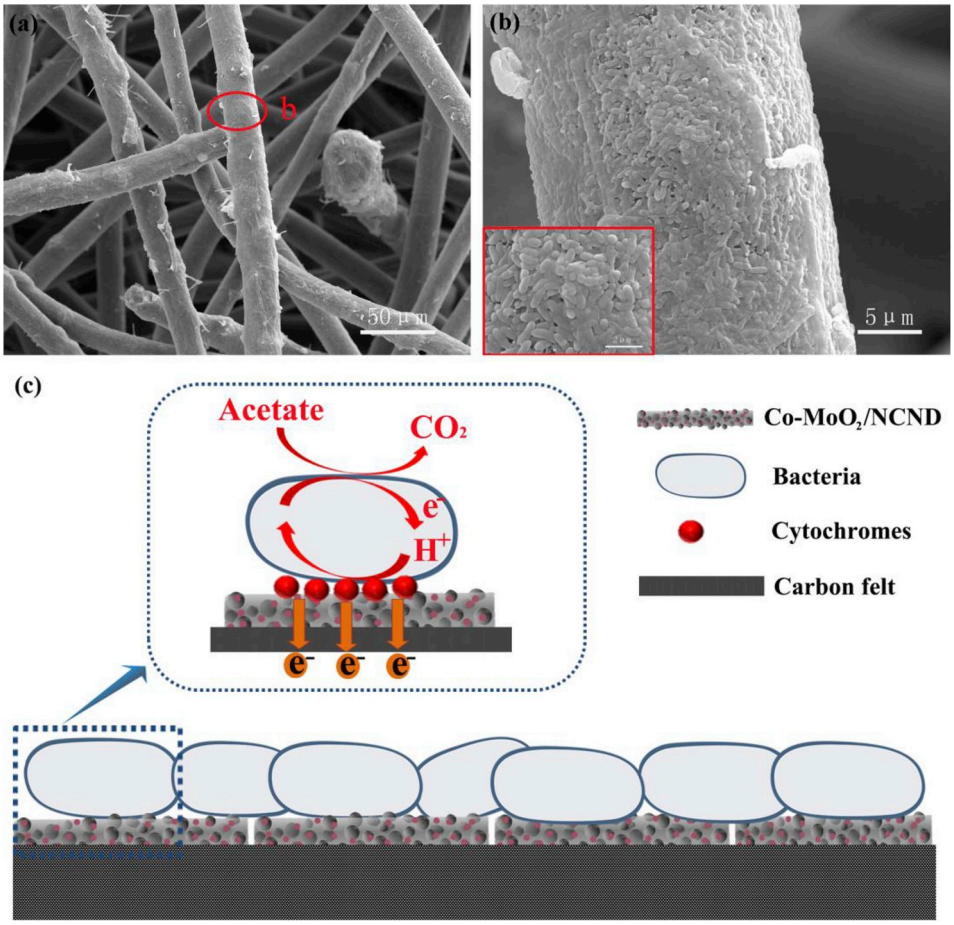

Fig. 6. SEM images (a, b) of the electroactive biofilm grown on Co–MoO_2/NCND/CF anode after one month's batch mode operations of MFCs at 25 °C; Schematic illustration on charge transfer mechanism between bacteria and Co–MoO_2/NCND/CF anode of MFC (c).

Declaration of competing interest

The authors declare that they have no known competing financial interests or personal relationships that could have appeared to influence the work reported in this paper.

CRediT authorship contribution statement

Xin Li: Investigation, Writing - original draft. **Meihua Hu:** Investigation, Writing - original draft. **Lizhen Zeng:** Investigation, Writing - original draft. **Juan Xiong:** Investigation, Writing - original draft. **Binhao Tang:** Investigation, Writing - original draft. **Zhangmin Hu:** Investigation, Writing - original draft. **Lidan Xing:** Supervision, Writing - review & editing. **Qiming Huang:** Supervision, Writing - review & editing. **Weishan Li:** Supervision, Writing - review & editing.

Acknowledgements

This work is financially supported by National Natural Science Foundation of China (Grant no. 51471073).

Appendix A. Supplementary data

Supplementary data to this article can be found online at https://doi.org/10.1016/j.bios.2019.111727.

References

Chen, X.F., Wang, X.S., Liao, K.T., Zeng, L.Z., Xing, L.D., Zhou, X.W., Zheng, X.W., Li, W. S., 2015. J. Mater. Chem. A 3, 19402–19409.
Cheng, S.A., Logan, B.E., 2007. Electrochem. Commun. 9, 492–496.
Cui, D., Wang, Y.Q., Xing, L.D., Li, W.S., 2014. Int. J. Hydrogen Energy 39, 15081–15087.
Fricke, K., Harnisch, F., Schröder, U., 2008. Energy Environ. Sci. 1, 144.
Guo, K., Freguia, S., Dennis, P.G., Chen, X., Donose, B.C., Keller, J., Gooding, J.J., Rabaey, K., 2013. Environ. Sci. Technol. 47, 7563–7570.
He, Z., Mansfeld, F., 2009. Energy Environ. Sci. 2, 215–219.
Hu, M.H., Li, X., Xiong, J., Zeng, L.Z., Huang, Y.S., Wu, Y.P., Cao, G.Z., Li, W.S., 2019. Biosens. Bioelectron. 142, 111594.
Jia, J., Tang, Y., Liu, B., Wu, D., Ren, N., Xing, D., 2013. Bioresour. Technol. 144, 94–99.
Katuri, K.P., Kavanagh, P., Rengaraj, S., Leech, D., 2010. Chem. Commun. (Camb) 46, 4758–4760.
Li, R., Wang, S., Wang, W., Cao, M., 2015. Phys. Chem. Chem. Phys. 17, 24803–24809.
Li, S., Cheng, C., Thomas, A., 2017. Adv. Mater. 29, 1602547.
Li, H., Liao, B., Xiong, J., Zhou, X., Zhi, H., Liu, X., Li, X., Li, W., 2018. J. Power Sources 379, 115–122.
Liao, L., Wang, S., Xiao, J., Bian, X., Zhang, Y., Scanlon, M.D., Hu, X., Tang, Y., Liu, B., Girault, H.H., 2014. Energy Environ. Sci. 7, 387–392.
Lin, H., Liu, N., Shi, Z., Guo, Y., Tang, Y., Gao, Q., 2016. Adv. Funct. Mater. 26, 5590–5598.
Liu, H., Ramnarayanan, R., Logan, B.E., 2004. Energy Environ. Sci. 38, 2281–2285.
Liu, Y., Harnisch, F., Fricke, K., Sietmann, R., Schroder, U., 2008. Biosens. Bioelectron. 24, 1012–1017.
Liu, Y., Zhang, H., Ouyang, P., Chen, W., Wang, Y., Li, Z., 2014. J. Mater. Chem. A 2, 4714–4721.
Logan, B.E., Rossi, R., Ragab, A., Saikaly, P.E., 2019. Nat. Rev. Microbiol. 17, 307–319.
Lovley, D.R., 2006. Nat. Rev. Microbiol. 4, 497.
Lv, Z., Xie, D., Yue, X., Feng, C., Wei, C., 2012. J. Power Sources 210, 26–31.
Mardanpour, M.M., Nasr Esfahany, M., Behzad, T., Sedaqatvand, R., 2012. Biosens. Bioelectron. 38, 264–269.
Mohamed, H.O., Abdelkareem, M.A., Obaid, M., Chae, S.H., Park, M., Kim, H.Y., Barakat, N.A.M., 2017. Chem. Eng. J. 326, 497–506.
Nevin, K.P., Kim, B.C., Glaven, R.H., Johnson, J.P., Woodard, T.L., Methe, B.A., Didonato, R.J., Covalla, S.F., Franks, A.E., Liu, A., Lovley, D.R., 2009. PLoS One 4, e5628.
Peng, L., Zhang, Y., 2017. Electrochim. Acta 228, 447–452.
Rabaey, Korneel, Lissens, Geert, Siciliano, Steven D., Verstraete, W., 2003. Biotechnol. Lett. 25, 1531–1535.
Richter, H., Nevin, K.P., Jia, H., Lowy, D.A., Lovley, D.R., Tender, L.M., 2009. Energy Environ. Sci. 2, 506.
Rosenbaum, M., Zhao, F., Quaas, M., Wulff, H., Schröder, U., Scholz, F., 2007. Appl. Catal., B 74, 261–269.
Rossi, R., Yang, W., Zikmund, E., Pant, D., Logan, B.E., 2018. Bioresour. Technol. 265, 200–206.
Wan, C., Leonard, B.M., 2015. Chem. Mater. 27, 4281–4288.
Wan, J., Wu, J., Gao, X., Li, T., Hu, Z., Yu, H., Huang, L., 2017. Adv. Funct. Mater. 27, 1703933.
Wang, Y., Li, B., Zeng, L., Cui, D., Xiang, X., Li, W., 2013. Biosens. Bioelectron. 41, 582–588.
Wang, Y., Li, B., Cui, D., Xiang, X., Li, W., 2014. Biosens. Bioelectron. 51, 349–355.
Wang, Y.Q., Huang, H.X., Li, B., Li, W.S., 2015. J. Mater. Chem. A 3, 5110–5118.
Wang, P., Zhang, Y., Yin, Y., Fan, L., Zhang, N., Sun, K., 2018. Chem. Eng. J. 334, 257–263.
Wang, R., Yan, M., Li, H., Zhang, L., Peng, B., Sun, J., Liu, D., Liu, S., 2018. Adv. Mater. 30, e1800618.
Watson, V.J., Logan, B.E., 2011. Electrochem. Commun. 13, 54–56.
Wu, X., Qiao, Y., Shi, Z., Tang, W., Li, C.M., 2018. ACS Appl. Mater. Interfaces 10, 11671–11677.
Xie, X., Criddle, C., Cui, Y., 2015. Energy Environ. Sci. 8, 3418–3441.
Xiong, J., Hu, M., Li, X., Li, H., Li, X., Liu, X., Cao, G., Li, W., 2018. Biosens. Bioelectron. 109, 116–122.
Yang, L.C., Sun, W., Zhong, Z.W., Liu, J.W., Gao, Q.S., Hu, R.Z., Zhu, M., 2016. J. Power Sources 306, 78–84.
Yang, L., Li, X., Ouyang, Y., Gao, Q., Ouyang, L., Hu, R., Liu, J., Zhu, M., 2016. ACS Appl. Mater. Interfaces 8, 19987–19993.
Yang, L., Yu, J., Wei, Z., Li, G., Cao, L., Zhou, W., Chen, S., 2017. Nano Energy 41, 772–779.
You, S., Ma, M., Wang, W., Qi, D., Chen, X., Qu, J., Ren, N., 2017. Adv. Energy Mater. 7, 1601364.
Yu, Y.Y., Guo, C.X., Yong, Y.C., Li, C.M., Song, H., 2015. Chemosphere 140, 26–33.
Yu, M., Cheng, X., Zeng, Y., Wang, Z., Tong, Y., Lu, X., Yang, S., 2016. Angew. Chem. Int. Ed. 55, 6762–6766.
Yuan, Y., Zhou, S., Liu, Y., Tang, J., 2013. Environ. Sci. Technol. 47, 14525–14532.
Zeng, L., Zhang, L., Li, W., Zhao, S., Lei, J., Zhou, Z., 2010. Biosens. Bioelectron. 25, 2696–2700.
Zeng, L., Chen, X., Li, H., Xiong, J., Hu, M., Li, X., Li, W., 2018. Electrochim. Acta 283, 528–537.
Zeng, L., Zhang, W., Xia, P., Tu, W., Ye, C., He, M., 2018. Biosens. Bioelectron. 102, 351–356.
Zhang, L., Zhou, S., Zhuang, L., Li, W., Zhang, J., Lu, N., Deng, L., 2008. Electrochem. Commun. 10, 1641–1643.
Zhang, H.J., Wang, K.X., Wu, X.Y., Jiang, Y.M., Zhai, Y.B., Wang, C., Wei, X., Chen, J.S., 2014. Adv. Funct. Mater. 24, 3399–3404.
Zhang, C., Liang, P., Jiang, Y., Huang, X., 2015. J. Power Sources 273, 580–583.
Zhang, Q., Zhang, Y., Li, D., 2017. Bioresour. Technol. 229, 104–110.
Zhong, Y., Pan, Z., Wang, X., Yang, J., Qiu, Y., Xu, S., Lu, Y., Huang, Q., Li, W., 2019. Adv. Sci. 1802243.
Zhou, M., Chi, M., Luo, J., He, H., Jin, T., 2011. J. Power Sources 196, 4427–4435.
Zhou, X., Chen, X., Li, H., Xiong, J., Li, X., Li, W., 2016. Electrochim. Acta 209, 582–590.
Zhou, S., Zhou, L., Zhang, Y., Sun, J., Wen, J., Yuan, Y., 2019. J. Mater. Chem. A 7, 4217–4229.
Zou, L., Qiao, Y., Wu, X.-S., Li, C.M., 2016. J. Power Sources 328, 143–150.
Zou, L., Huang, Y., Wu, X., Long, Z., 2019. J. Power Sources 413, 174–181.